Spin density waves in the Hubbard model: A DMFT approach

Robert Peters[1,2,*] and Norio Kawakami[1]
[1]*Department of Physics, Kyoto University, Kyoto 606-8502, Japan*
[2]*Computational Condensed Matter Physics Laboratory, RIKEN, Wako, Saitama 351-0198, Japan*
(Received 17 March 2014; revised manuscript received 13 April 2014; published 24 April 2014)

We analyze spin density waves (SDWs) in the Hubbard model on a square lattice within the framework of inhomogeneous dynamical mean field theory (IDMFT). Doping the half-filled Hubbard model results in a change of the antiferromagnetic Néel state, which exists exactly at half filling, to a phase of incommensurate SDWs. Previous studies of this phase mainly rely on static mean field calculations. In this paper, we will use large-scale IDMFT calculations to study properties of SDWs in the Hubbard model. A great advantage of IDMFT over static mean field approaches is the inclusion of local screening effects and the easy access to dynamical correlation functions. Furthermore, this technique is not restricted to the Hubbard model, but can be easily used to study incommensurate phases in various strongly correlated materials.

DOI: 10.1103/PhysRevB.89.155134 PACS number(s): 71.10.Fd, 75.10.−b, 75.30.Fv

I. INTRODUCTION

Strongly correlated materials have been the focus of interest for over half a century, because of their intriguing properties such as metal-insulator transitions, magnetism, and high-temperature superconductivity, which cannot be observed in weakly interacting systems. A prototype model for theoretically describing strongly correlated materials is the one-band Hubbard model [1–3],

$$H = \sum_{ij,\sigma} t_{ij} c^{\dagger}_{i\sigma} c_{j\sigma} + U \sum_{i} n_{i\downarrow} n_{i\uparrow}, \tag{1}$$

where the first term corresponds to the kinetic energy and the second term to a local density-density interaction. The operator $c^{\dagger}_{i\sigma}$ creates an electron on lattice site i in spin direction σ, and the operator $n_{i\sigma} = c^{\dagger}_{i\sigma} c_{i\sigma}$ corresponds to the electron density at site i. The interaction is taken to be repulsive, $U > 0$, throughout this paper.

The physics of the Hubbard model with repulsive interaction is determined by the competition between the local density-density interaction and the nonlocal kinetic energy. This competition is the cause for the Mott-metal-insulator transition, a well known phenomenon observed in the Hubbard model [4]. The half-filled Hubbard model undergoes a transition from a metal to a Mott insulator, where, due to the repulsive interaction, electrons become localized. Besides the metal-insulator transition, long-range ordered phases have also been extensively studied in the Hubbard model. For a bipartite lattice and large enough dimensions, $d > 1$, the ground state of the Hubbard model at half filling is an antiferromagnetic Néel state; each lattice site is occupied with one electron in average, and the spin polarization alternates between neighboring lattice sites. Besides this antiferromagnetic phase at half filling, one can also observe different ordered phases such as ferromagnetism or superconductivity in the Hubbard model, depending on the lattice structure and system parameters.

There are a variety of analytical and numerical techniques to theoretically analyze the Hubbard model. A particularly successful technique, which is able to directly study the properties of strongly correlated models, is the dynamical mean field theory (DMFT) [5–7]. DMFT maps the lattice model onto a quantum impurity model, which must be solved self-consistently. Nonlocal terms in the self-energy are thereby neglected, which becomes exact for infinite dimensional lattices. Although DMFT is an approximation for real materials, it has provided many insights into fundamental properties of strongly correlated materials. Furthermore, there are ways to incorporate the momentum dependence into the self-energy, which are known as cluster DMFT or dynamical cluster approximation [8].

Although long-range ordered phases have been analyzed by DMFT since the introduction of the method, previous works have mainly focused on commensurate phases such as the antiferromagnetic Néel state, ferromagnetism, etc. In order to analyze the antiferromagnetic Néel state within DMFT [9–15], the lattice is divided into two-site clusters, and momentum-independent self-energies are calculated separately for each sublattice. This method is known as the two-sublattice method.

The antiferromagnetic state with electron density close to, but away from unity has little been analyzed within DMFT. One approach to perform DMFT calculations for such incommensurate states has been to incorporate a fixed rotation angle of the spin direction into the DMFT equations [16,17]. However, if the assumed rotation angle does not correspond to the ground state of the system, or if one performs a usual two-sublattice DMFT calculation for the doped Hubbard model, the self-energy oscillates during the self-consistency calculation and a converged solution cannot be obtained. We previously interpreted these oscillations as the tendency of the system to form a spin density wave (SDW) [14,15]. However, this interpretation was mathematically not well founded and properties of the SDW state could not be determined, because the DMFT calculation did not converge.

In this paper, we demonstrate how to overcome these above-mentioned difficulties by performing large-scale simulations using the inhomogeneous DMFT (IDMFT) to study inhomogeneous phases in strongly correlated materials. As an example, we study incommensurate SDW states in the doped Hubbard model on a square lattice. However, the IDMFT is

*peters@scphys.kyoto-u.ac.jp

neither restricted to the Hubbard model nor to the square lattice, but can be employed for any strongly correlated model with local interactions. We show that the oscillations, which have been observed in previous DMFT calculations, indeed indicate the emergence of SDWs. The IDMFT is an extension of DMFT to incorporate inhomogeneities and has been so far used to study surfaces, interfaces, superlattices, and trapped strongly correlated systems [18–28]. Furthermore, there have been a few works in which the IDMFT has been used for SDWs in the Hubbard model. However, these calculations have been for small cluster sizes or one-dimensional slices of the lattice. Thus, these calculations mainly focused on the SDW state called vertical stripes in the context of the high-temperature superconducting cuprates [29–31]. Using the IDMFT, we are able to find a converged and self-consistent solution for the doped, magnetically ordered Hubbard model, and thus are able to analyze different kinds of SDWs without *a priori* knowing the rotation angle of the SDW. Furthermore, the IDMFT gives us a direct access to dynamical correlation functions, which is a great advantage over previous static mean field calculations.

The remainder of this paper is organized as follows: In the next section, we will explain technical details of the IDMFT calculations. This is followed by our results for the SDW phase of the Hubbard model, including an analysis of static as well as dynamical properties. A short summary will conclude this paper.

II. TECHNICAL DETAILS ON THE CALCULATIONS

A. Dynamical mean field theory

DMFT relates the lattice model to a quantum impurity model. This mapping becomes exact in the limit of infinite dimensions. In this high-dimensional limit, the hopping amplitude has to be scaled as $t \to t^\star/\sqrt{z}$ (z is the coordination number of the lattice), in order to ensure a nontrivial kinetic energy. A consequence of this scaling is the vanishing of the momentum dependence of the self-energy, $\Sigma(k,\omega) \to \Sigma(\omega)$.

The local lattice Green's function can thus be written as

$$G_{\mathrm{loc}}(z) = \frac{1}{N}\sum_k \frac{1}{z-\epsilon_k-\Sigma(z)} = \int d\epsilon \frac{\rho_0(\epsilon)}{z-\epsilon-\Sigma(z)}, \tag{2}$$

where ϵ_k represents the noninteracting band structure of the lattice, and $\rho(\epsilon)$ the corresponding noninteracting local density of states (DOS).

The mapping onto a quantum impurity model can be done by comparing the local lattice Green's function [Eq. (2)] to the Green's function of an impurity model with the same local interaction term, which reads

$$G_{\mathrm{imp}}(z) = \frac{1}{z-\Delta(z)-\Sigma(z)},$$

where $\Delta(z)$ is the hybridization between the impurity level and an electron bath.

An iteratively performed DMFT calculation is done as follows: First, with a given self-energy, which can be zero in the first iteration, the local lattice Green's function is calculated by Eq. (2). Second, from this local lattice Green's function, one calculates the hybridization $\Delta(z)$ of the corresponding quantum impurity model by

$$\Delta(z) = z - [G_{\mathrm{loc}}(z)]^{-1} - \Sigma(z). \tag{3}$$

This hybridization defines a quantum impurity model, whose self-energy must be determined. With this self-energy, one calculates a new local lattice Green's function from which the next quantum impurity model is determined. This procedure continues until a converged solution is found.

The DMFT can also be used to investigate properties of long-range ordered phases of strongly correlated models. When performing calculations for a magnetic phase, one has to calculate a spin-dependent self-energy, which results in a spin-dependent hybridization of the quantum impurity model. In the case of an antiferromagnetic Néel state, one has to take into account the doubling of the unit cell. The local lattice Green's function can then be calculated by the so-called *AB*-sublattice method,

$$G_{\mathrm{loc}}(z) = \int d\epsilon \rho_0(\epsilon) \begin{pmatrix} z-\Sigma_\uparrow(z) & -\epsilon \\ -\epsilon & z-\Sigma_\downarrow(z) \end{pmatrix}^{-1}.$$

As stated above, the *AB*-sublattice method works well for the antiferromagnetic Néel state, where the spin direction alternates between nearest neighbors. However, this method fails to describe long-range ordered phases, which are not commensurate with two sublattices, e.g., the antiferromagnetic state of the doped Hubbard model. In the following, we will show how to overcome this problem by using IDMFT.

B. IDMFT for SDWs

In order to stabilize a long-range ordered SDW state with wavelength larger than two lattice sites, one has to divide the lattice into large enough clusters so that the wavelength of the ordered state can be taken correctly into account. A way to do that is to use the IDMFT, which maps each lattice site of a cluster onto its corresponding quantum impurity model, thereby assuming a momentum-independent self-energy. Although the self-energy between different lattice sites vanishes within this approximation, the self-energy of each lattice site may be different. The IDMFT can thus describe inhomogeneous systems, such as cold atoms in a trap potential, or interfaces and surfaces of strongly correlated systems. We here apply the IDMFT for a homogeneous model, but in a situation where the symmetry of the model is spontaneously broken, which results in an inhomogeneous state.

The IDMFT works as follows: After setting the size of our cluster, usually between 400 and 2000 lattice sites, we initialize a self-energy for each lattice site. In the first DMFT iteration, this self-energy can be set to zero. We usually choose this self-energy in a way that it breaks the SU(2) symmetry of the Hamiltonian in order to obtain an SDW wave solution. [If the SU(2) symmetry is not broken, the IDMFT solution will be a paramagnetic state.] Using these self-energies, we calculate the local Green's functions for all lattice sites by using a matrix inversion:

$$\mathbf{G}_{\mathrm{loc}}(z) = [z\cdot\mathbb{I} - \mathbf{H} - \Sigma]^{-1}, \tag{4}$$

where $\mathbf{H}$ is the noninteracting Hamiltonian of the chosen cluster. At this point, one must specify if the calculation is performed for a finite cluster with open or periodic boundary conditions, or if the calculation is for an infinite lattice, which consists of repeating this finite cluster. In the case of the infinite lattice, the Hamiltonian will include momentum-dependent terms, which must be integrated over. Equation (4) then reads

$$\mathbf{G}_{\mathrm{loc}}(z) = \int dk_x dk_y ([z \cdot \mathbb{I} - \mathbf{H}_{k_x,k_y} - \Sigma]^{-1}).$$

After having calculated all local Green's functions, lattice-site-dependent quantum impurity models can be determined similar to Eq. (3) by

$$\Delta_{ii}(z) = z - [G_{ii,\mathrm{loc}}(z)]^{-1} - \Sigma_{ii}(z). \tag{5}$$

(The inversion of the local Green's function is performed locally in order to determine the hybridization of a local quantum impurity model.) We now solve all these quantum impurity models and calculate the corresponding self-energies. With these self-energies, one can then calculate the local Green's function of the next IDMFT iteration [see Eq. (4)]. Because the self-energy depends on the lattice site, this method is able to calculate properties of inhomogeneous phases for this cluster.

During the IDMFT procedure, self-energies of several quantum impurity models must be calculated. In this paper, we use the numerical renormalization group (NRG) [32,33] for this purpose. The NRG is a well established method which is able to calculate numerical-exact dynamical correlation functions such as Green's functions and self-energies [34,35].

These calculations thereby involve two time consuming steps: First is the calculation of the self-energies of all lattice sites, which scales linearly with the number of lattice sites. The other time consuming step is the calculation of the local Green's functions, which involves a matrix inversion of the whole cluster and thus scales cubically with the number of lattice sites.

Although we are using a cluster of lattice sites in our calculations, IDMFT is fundamentally different from the cluster DMFT (CDMFT) or the dynamical cluster approximation (DCA) [8]. In IDMFT, one determines a local self-energy separately for all lattice sites, while in the latter methods, one solves a multisite impurity model for the whole cluster, thus determining also nonlocal terms of the self-energy. Therefore, the CDMFT and the DCA are more accurate in principle, because they incorporate nonlocal fluctuations. However, a cluster of approximately 1000 sites is by far out of range for these methods.

III. DOPED ANTIFERROMAGNETIC STATE IN THE HUBBARD MODEL

Intensive studies about incommensurate SDW states in the Hubbard model began approximately at the same time as the discovery of high-temperature superconductivity [36] that appears in strongly correlated materials close to an antiferromagnetic phase [37]. These studies concerned the antiferromagnetic phases in the t-J model [38–45] and the Hubbard model [10,16,17,46–63] and mainly exploited different types of static mean field theory, e.g., Hartree-Fock theory. Summarizing these results, one can say that an extended region of SDW states exists in the phase diagram of the Hubbard model close to half filling. At weak coupling, these SDWs run along one axis in the (0,1) or (1,0) direction, which are called vertical SDWs. For stronger coupling, the energetically favored state is an SDW running along the diagonal of the square lattice. Furthermore, the SDW state is accompanied by a charge density wave in the same direction. For strong enough coupling, the doped holes localize in straight lines, yielding large areas of nearly half-filled antiferromagnetically ordered sites and paramagnetic stripes with a particle number of less than one. These states are usually referred to as stripe- or domain-wall states. As already mentioned above, besides these static mean field calculations, there have been up to now only a few DMFT calculations, because the two-sublattice method does not yield a converged solution for the doped Hubbard model. There have been IDMFT calculations for small clusters, mainly one-dimensional (1D) cuts through the two-dimensional (2D) lattice [29–31], or DMFT calculations incorporating knowledge about properties of the SDW [16,17], such as the ordering vector. Furthermore, we want to note that there have been some density matrix renormalization group [64–68] and constraint-path quantum Monte Carlo calculations [64,69] for stripes in the doped Hubbard model. However, these simulations are also restricted to small cluster sizes.

In contrast to these previous approaches, we here use the IDMFT for large clusters of lattice sites. This allows us to stabilize different kinds of SDWs without knowledge about their properties, such as an ordering wave vector. Furthermore, the IDMFT incorporates local fluctuations exactly and thus goes well beyond static mean field theory and gives a direct access to dynamical properties, i.e., Green's functions and self-energies.

We have performed IDMFT calculations for a finite cluster of at least 400 and up to 2000 lattice sites using periodic boundary conditions. In these calculations, we have found, in accordance with previous static mean field calculations, that doping the antiferromagnetic Néel state in the Hubbard model results in SDW states. A typical solution of such an SDW state is shown in Fig. 1. The upper (lower) panel shows the polarization (occupation) of the lattice. In agreement with previous calculations, we see that the SDW is accompanied by a charge density wave in the same direction. The polarization of the electrons thereby depends on the electron density. Regions of large electron density, which exhibit a Néel-state-like order with large polarization, are separated by regions of low electron density, which exhibit only a small polarization or are magnetically disordered. For strong interaction, these regions of low electron density form narrow straight lines, which have been previously called stripes. In Fig. 1, we observe that exactly at the center of these stripes, there are always two neighboring sites which are ferromagnetically aligned. Thus, the Néel states of neighboring high electron-density regions are phase shifted. This is in accordance with previous calculations.

In Fig. 2, we summarize our calculations in a phase diagram of the Hubbard model including SDW states. For weak interaction strengths, $U < 3t$, we do not observe any SDW phase. However, for these weak interactions, the antiferromagnetic Néel state can be slightly doped without destroying the Néel order and exists up to $n \approx 0.97$ electrons

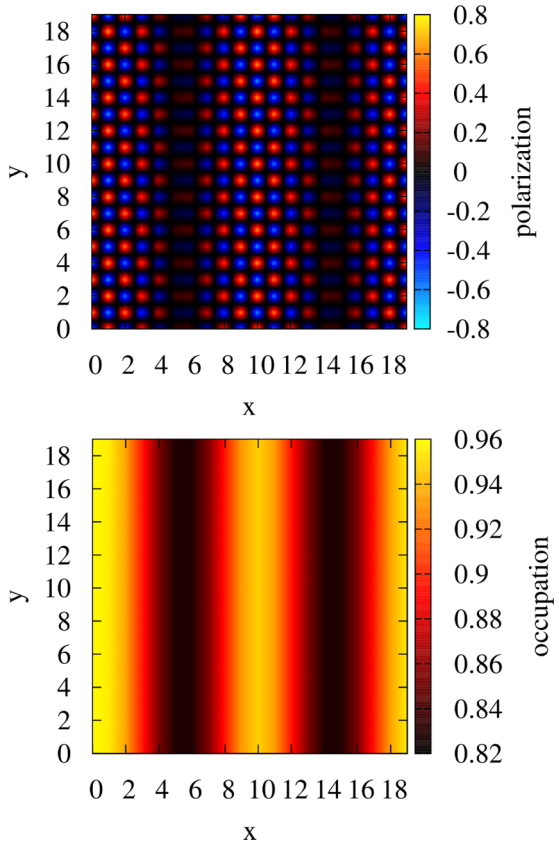

FIG. 1. (Color online) Typical pattern for a vertical SDW state in the Hubbard model for $U = 8t$ and an average electron density $\langle n \rangle = 0.9$. The upper (lower) panel shows the electron polarization (density).

per lattice. For $U > 3t$, doping the Néel state results in the emergence of SDW states in the Hubbard model. We have mainly focused on vertical SDW states, which run along

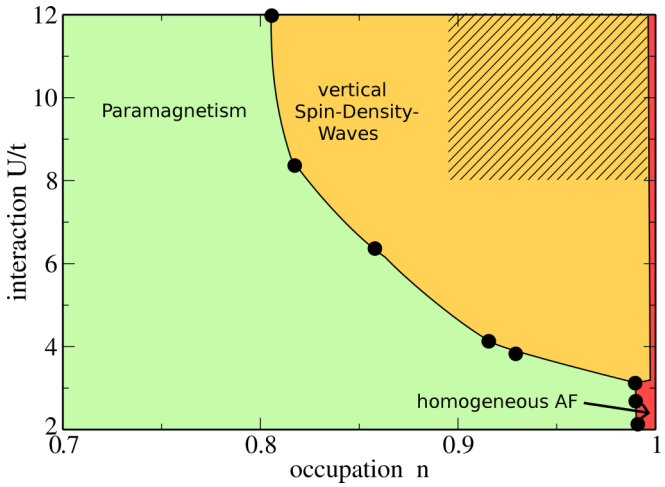

FIG. 2. (Color online) Phase diagram of the Hubbard on a square lattice as calculated by IDMFT. The shaded region represents parameters where we find vertical as well as diagonal SDWs to be stable. The homogeneous Néel state exists exactly at half filling for all interaction strengths and for a slightly doped region at weak interaction.

one of the axes of the square lattice (see, e.g., Fig. 1). These states have been identified by previous Hartree-Fock calculations as the ground state in the Hubbard model for moderate interaction strengths. In our calculations, these SDW states are stable for strong enough interactions up to an electron density $n \approx 0.8$. Compared to previous static mean field calculations, our calculated critical occupation number is much closer to unity. This can be explained by quantum fluctuations which are included in IDMFT but are absent in static mean field calculations. The local interaction is screened by these quantum fluctuations. Thus, static mean field theories overestimate the parameter region of ordered states. We want to point out that besides the vertical SDW, different types of SDWs can be observed in IDMFT calculations. In the whole parameter regime where vertical SDW states are stable, SDW states which do not break the square-lattice symmetry can also be observed. These symmetric SDWs consist of modulations which run along both diagonals of the square lattice. Furthermore, for strong interactions, $U/t > 7t$, diagonal SDW states which run along a single diagonal of the square lattice can be observed close to half filling. The shaded region in Fig. 2 corresponds to parameters where we find diagonal SDW states to be stable. These diagonal SDW states are unstable for weak interaction strengths and large doping. All stabilized SDW states are energetically very close to each other; energetic differences are below our current accuracy. However, compared to the paramagnetic state, any of these SDW states is lower in energy.

Which state is realized in our IDMFT calculations depends not only on the energy of the state but also on the way how the symmetry is broken during the IDMFT calculation. If the SU(2) symmetry is not broken at all, a paramagnetic state is formed. If the SU(2) symmetry is broken at a single point, e.g., by applying a magnetic field in the first IDMFT iteration at a single lattice site, then a square-lattice-symmetric state arises. If a magnetic field is applied to lattice sites in a vertical (diagonal) line, a vertical (diagonal) SDW arises, if energetically stable.

In order to present a more detailed analysis of SDW states, we focus now on the vertical SDW state. Our results about vertical SDW states are summarized in Fig. 3. In Figs. 3(a) and 3(b), we show the spatial modulation of the electron density and the spin polarization for different occupation numbers and interaction strengths. The period of the modulation increases with increasing average electron density (the closer the average occupation is to unity, the longer is the period). This is confirmed in Fig. 3(b), where we show that the period of the modulation is approximately the inverse of the average number of holes per lattice site, $p = 1/(1 - n)$, where n is the average number of electrons. Moreover, in Fig. 3(a) it is visible that while for low average electron densities the modulation is sinelike, the maximum is flattened, if the occupation is close to unity; there are more and more half-filled lattice sites that exhibit a Néel-state-like order, while holes are located within narrow walls. These states have been called domain-wall states or stripes in previous mean field calculations. While the period of the modulation strongly depends on the average electron density, it is independent of the interaction strength. For increasing the interaction value for a fixed occupation number [Figs. 3(c) and 3(d)], the amplitude of the modulation

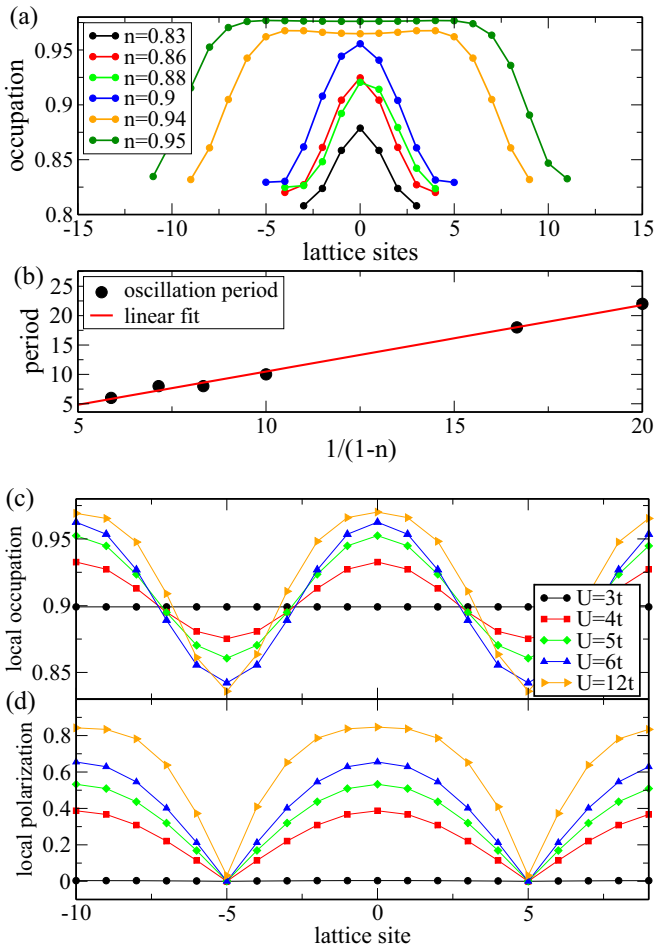

FIG. 3. (Color online) (a) Electron density against lattice sites for different average electron densities and $U = 8t$. We only show a single oscillation of the electron density which is periodically continued. (b) The extracted period of the modulation of the electron density against the reciprocal density of holes, $1/(1-n)$ (n is the average number of electrons per lattice site). (c) Electron density against lattice sites for different interaction strengths and fixed average electron density $n = 0.9$. (d) The magnitude of the spin polarization, $P = |n_\uparrow - n_\downarrow|$, against different lattice sites for different interaction strengths.

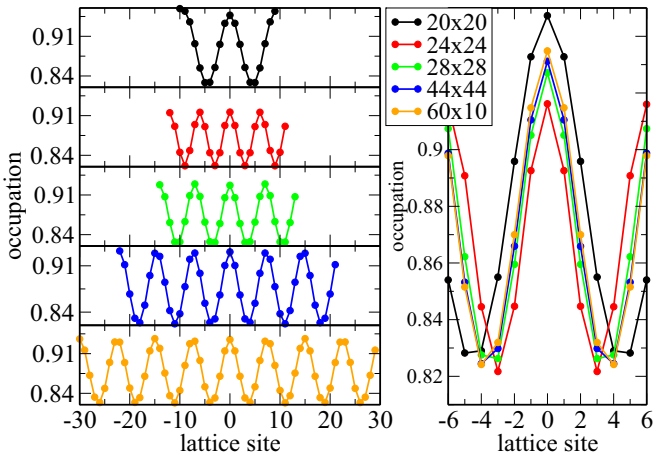

FIG. 4. (Color online) Left: Occupation number of different lattice sites of a vertical SDW for a fixed chemical potential and interaction strength but different cluster sizes. Right: Direct comparison of a single period of the SDW for different cluster sizes. (The colors of the right panel correspond to the colors of the left panels.)

becomes larger, and thus the SDW becomes more stripelike. The maximum of the local electron density increases while the minimum decreases. At the same time, also the maximum of the electron polarization increases. However, the modulation period remains unchanged, if the average filling of the lattice is not changed. These static properties of SDW states, such as amplitude and modulation period, qualitatively agree with previous static mean field calculations.

In contrast to previous attempts to use DMFT, we are here using large-scale IDMFT calculations. We are thus able to analyze the influence of finite size effects on our calculations. Because of the usage of periodic boundary conditions, an integer number of oscillations of the SDW must be included within the cluster. If the cluster size does not match the period of the energetically most stable SDW, which is related to the occupation number of the system, two things may happen in the system: First, the period of the SDW may be slightly modified. Second, while most oscillations of the SDW within the cluster correspond to the most stable SDW, there are a few oscillations which are altered in order to accommodate the SDW within the cluster. Figure 4 shows the occupation profiles of vertical SDWs for interaction strength $U = 8t$ and chemical potential $\mu = 2t$ for different cluster sizes. The left panels show the occupation number of different lattice sites of the SDW for different cluster sizes. These panels show that the qualitative structure of the SDW does only weakly depend on the cluster size. A direct comparison of a single oscillation of the SDWs on these different clusters is presented in the right panel of Fig. 4. The average occupation for this chemical potential is approximately $\langle n \rangle = 0.875$, corresponding to an SDW with period 8. We here show a comparison of an oscillation in the middle of our cluster, where we have initially broken the SU(2) symmetry and thus the SDW is usually best converged within the cluster. We observe that while the SDWs for the clusters 20×20 and 24×24 have different periods and different amplitudes of the occupation, the SDWs for cluster sizes larger than 28 and the rectangular cluster look very similar. The size of the cluster which is needed to obtain reliable results does of course depend on the period of the SDW. We observe that the cluster size should be approximately four times the period of the SDW, which makes it more and more difficult to calculate SDWs close to half filling with very long periods.

An advantage of IDMFT over static mean field calculations is the easy access to dynamical properties; in fact, dynamical properties such as self-energies are calculated in order to perform an IDMFT procedure. It should be noted that the Green's function takes two lattice sites as indices, $G_{(x_1,y_1),(x_2,y_2)}$, because properties vary among different lattice sites. Therefore, the Green's function cannot be written in terms of the distance between lattice sites. However, in order to show a DOS which does only depend on a single momentum $\vec{k} = (k_x, k_y)$, we Fourier transform the distance of lattice sites, $\vec{d} = (x_1 - x_2, y_1 - y_2)$, and average it over the whole

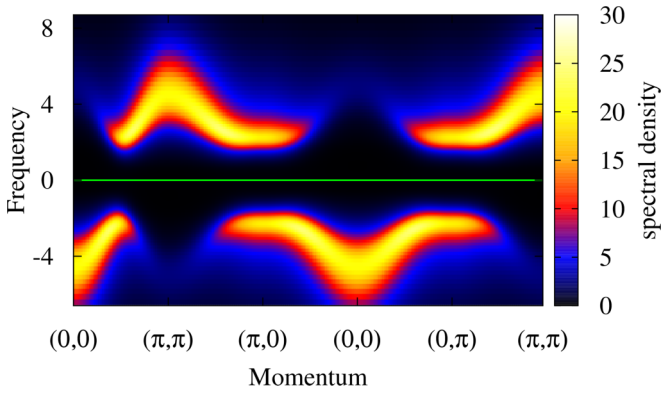

FIG. 5. (Color online) Momentum-resolved spectral function for the half-filled Hubbard model for $U = 8t$. The green line marks the Fermi energy.

lattice. The resulting momentum-resolved spectral function corresponds then to the DOS which would be measured, e.g., in angle-resolved photoemission spectroscopy. We thus calculate

$$G_{k_x,k_y}(\omega) = \frac{1}{N}\sum_{x_1,y_1}\sum_{x_2,y_2}\{G_{(x_1,y_1),(x_2,y_2)}(\omega) \times \exp[i(k_x(x_1-x_2)+k_y(y_1-y_2))]\}.$$

The momentum-resolved spectral functions shown below are then given by $\rho_{k_x,k_y}(\omega) = -\frac{1}{\pi}\mathrm{Im}[G_{k_x,k_y}(\omega)]$.

The momentum-resolved DOS of a half-filled Hubbard model for $U = 8t$ is shown in Fig. 5. The system is in an insulating antiferromagnetic Néel state. The DOS exhibits a gap around the Fermi energy, as denoted by the green line. If we dope holes into the system, this state changes into a vertical SDW state. The momentum-resolved DOS for a vertical SDW with average electron density $\langle n\rangle = 0.95$ is shown in Fig. 6. We observe that the lower band crosses the Fermi energy at three points in momentum space: $\vec{k} = (\pi/2,\pi/2)$, $\vec{k} = (0,\pi)$, and $\vec{k} = (\pi,0)$. In a magnification of the DOS around the Fermi energy (lower panel of Fig. 6), however, we see that the band which crosses the Fermi energy becomes gapped at $\vec{k} = (\pi/2,\pi/2)$ and $\vec{k} = (0,\pi)$. There is a small but finite gap at the Fermi energy. The lower band possesses spectral weight only for $\vec{k} = (\pi,0)$ at the Fermi energy. This "pseudogap" originates in the SDW order. In the vertical SDW state, which is shown in Fig. 6, the spectrum becomes gapped for $\vec{k} = (\pi/2,\pi/2)$ and one of the two momenta, $\vec{k} = (\pi,0)$ or $\vec{k} = (0,\pi)$, depending on the direction of the vertical SDW. The momentum where the spectrum at the Fermi energy is not gapped thereby corresponds to the direction of the SDW; if there is spectral weight at the Fermi energy for $\vec{k} = (\pi,0)$, then the SDW runs along the x directions. This means that there are paramagnetic stripes in the y direction. These paramagnetic stripes are the cause for the spectral weight at the momentum $\vec{k} = (\pi,0)$. For comparison, we show the spectral function of the square-lattice-symmetric SDW state in Fig. 7. Due to symmetry, the spectral weight around $\vec{k} = (\pi,0)$ and $\vec{k} = (0,\pi)$ is equal. Furthermore, both momenta possess spectral weight at the Fermi energy. The spectrum only becomes gapped at the Fermi energy for $\vec{k} = (\pi/2,\pi/2)$. We can therefore say that this pseudogap in the spectral function is clearly related to the SDW order.

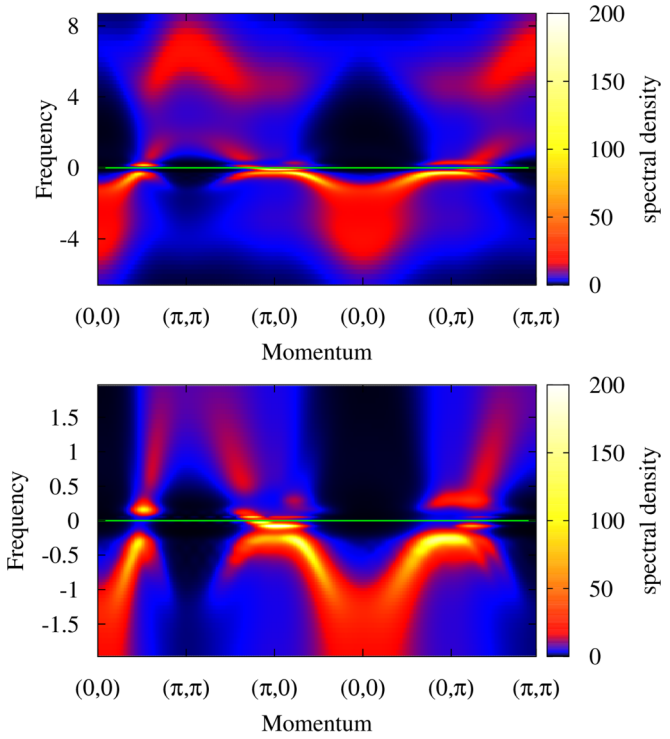

FIG. 6. (Color online) Momentum-resolved spectral function for the doped Hubbard model for $U = 8t$, $\langle n\rangle = 0.95$ in the vertical SDW state. The green line marks the Fermi energy. The lower panel is a magnification around the Fermi energy.

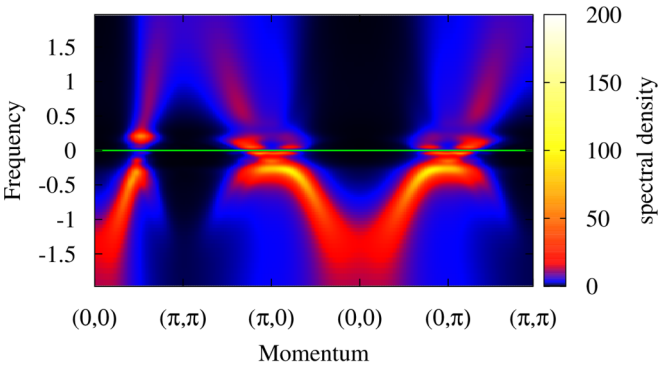

FIG. 7. (Color online) Momentum-resolved spectral function for the doped Hubbard model for $U = 8t$, $\langle n\rangle = 0.95$ in the square-lattice-symmetric SDW state. The green line marks the Fermi energy.

IV. CONCLUSIONS

We have used the IDMFT for the calculation of incommensurate SDW states in strongly correlated electron systems such as the Hubbard model and have thereby resolved difficulties encountered in previous DMFT treatments of magnetic states away from half filling. We have calculated the magnetic phase diagram of the Hubbard model on a square lattice including SDW states, and have shown that screening of the Coulomb interaction due to local fluctuations, which cannot be taken into account in static mean field calculations, strongly modifies

the phase diagram. As a result, magnetically ordered phases vanish for average electron densities $n < 0.8$. We have focused in this paper on vertical SDWs, although different types of SDW can be stabilized. The calculated properties, such as the period of the SDW, agree very well with previous calculations. However, a great advantage of IDMFT over static mean field calculations is the easy access to dynamical properties such as momentum-resolved spectral functions. We have shown that due to the SDW order, parts of the spectrum at the Fermi energy become gapped. The Fermi momenta at which the spectrum is gapped are directly related to the type of SDW state, e.g., in which direction the vertical SDW runs.

Finally, we want to stress that this method is not limited to the SDWs in the Hubbard on a square lattice, but can also be used for studying properties of incommensurate ordered phases for various 2D as well as three-dimensional (3D) lattices. Furthermore, it can be easily adopted to study different strongly correlated models as long as the interaction is local.

ACKNOWLEDGMENTS

R.P. and N.K. thank the Japan Society for the Promotion of Science (JSPS) for the support through its FIRST Program. R.P. thanks RIKEN for the support through the FPR program. N.K. acknowledges support through KAKENHI (No. 22103005 and No. 25400366). The numerical calculations were performed at the ISSP in Tokyo and on the SR16000 at YITP in Kyoto University.

[1] J. Hubbard, Proc. R. Soc. London, Ser. A **276**, 238 (1963).
[2] J. Kanamori, Prog. Theor. Phys. **30**, 275 (1963).
[3] M. C. Gutzwiller, Phys. Rev. Lett. **10**, 159 (1963).
[4] M. Imada, A. Fujimori, and Y. Tokura, Rev. Mod. Phys. **70**, 1039 (1998).
[5] W. Metzner and D. Vollhardt, Phys. Rev. Lett. **62**, 324 (1989).
[6] T. Pruschke, M. Jarrell, and J. Freericks, Adv. Phys. **44**, 187 (1995).
[7] A. Georges, G. Kotliar, W. Krauth, and M. J. Rozenberg, Rev. Mod. Phys. **68**, 13 (1996).
[8] T. Maier, M. Jarrell, T. Pruschke, and M. H. Hettler, Rev. Mod. Phys. **77**, 1027 (2005).
[9] M. Jarrell, Phys. Rev. Lett. **69**, 168 (1992).
[10] J. K. Freericks and M. Jarrell, Phys. Rev. Lett. **74**, 186 (1995).
[11] P. G. J. van Dongen, Phys. Rev. Lett. **74**, 182 (1995).
[12] P. G. J. van Dongen, Phys. Rev. B **54**, 1584 (1996).
[13] R. Zitzler, T. Pruschke, and R. Bulla, Eur. Phys. J. B **27**, 473 (2002).
[14] R. Peters and T. Pruschke, Phys. Rev. B **79**, 045108 (2009).
[15] R. Peters and T. Pruschke, New J. Phys. **11**, 083022 (2009).
[16] M. Fleck, A. I. Liechtenstein, A. M. Oleś, L. Hedin, and V. I. Anisimov, Phys. Rev. Lett. **80**, 2393 (1998).
[17] M. Fleck, A. I. Lichtenstein, A. M. Oleś, and L. Hedin, Phys. Rev. B **60**, 5224 (1999).
[18] M. Potthoff and W. Nolting, Phys. Rev. B **59**, 2549 (1999).
[19] R. W. Helmes, T. A. Costi, and A. Rosch, Phys. Rev. Lett. **101**, 066802 (2008).
[20] M. Snoek, I. Titvinidze, C. Töke, K. Byczuk, and W. Hofstetter, New J. Phys. **10**, 093008 (2008).
[21] H. Zenia, J. K. Freericks, H. R. Krishnamurthy, and T. Pruschke, Phys. Rev. Lett. **103**, 116402 (2009).
[22] E. V. Gorelik, I. Titvinidze, W. Hofstetter, M. Snoek, and N. Blümer, Phys. Rev. Lett. **105**, 065301 (2010).
[23] M. Snoek, I. Titvinidze, and W. Hofstetter, Phys. Rev. B **83**, 054419 (2011).
[24] Y. Tada, R. Peters, M. Oshikawa, A. Koga, N. Kawakami, and S. Fujimoto, Phys. Rev. B **85**, 165138 (2012).
[25] R. Peters, Y. Tada, and N. Kawakami, Phys. Rev. B **88**, 155134 (2013).
[26] Y. Tada, R. Peters, and M. Oshikawa, Phys. Rev. B **88**, 235121 (2013).
[27] M. O. J. Heikkinen, D.-H. Kim, and P. Törmä, Phys. Rev. B **87**, 224513 (2013).
[28] R. Peters and N. Kawakami, Phys. Rev. B **89**, 041106 (2014).
[29] M. Fleck, A. I. Lichtenstein, E. Pavarini, and A. M. Oleś, Phys. Rev. Lett. **84**, 4962 (2000).
[30] M. Fleck, A. I. Lichtenstein, and A. M. Oleś, Phys. Rev. B **64**, 134528 (2001).
[31] M. Raczkowski and F. F. Assaad, Phys. Rev. B **82**, 233101 (2010).
[32] K. Wilson, Rev. Mod. Phys. **47**, 773 (1975).
[33] R. Bulla, T. Costi, and T. Pruschke, Rev. Mod. Phys. **80**, 395 (2008).
[34] R. Peters, T. Pruschke, and F. B. Anders, Phys. Rev. B **74**, 245114 (2006).
[35] A. Weichselbaum and J. von Delft, Phys. Rev. Lett. **99**, 076402 (2007).
[36] J. Bednorz and K. Müller, Z. Phys. B: Condens. Matter **64**, 189 (1986).
[37] P. W. Anderson, Science **235**, 1196 (1987).
[38] B. I. Shraiman and E. D. Siggia, Phys. Rev. Lett. **62**, 1564 (1989).
[39] B. I. Shraiman and E. D. Siggia, Phys. Rev. Lett. **61**, 467 (1988).
[40] C. L. Kane, P. A. Lee, T. K. Ng, B. Chakraborty, and N. Read, Phys. Rev. B **41**, 2653 (1990).
[41] D. Yoshioka, J. Phys. Soc. Jpn. **58**, 1516 (1989).
[42] J.-i. Igarashi and P. Fulde, Phys. Rev. B **45**, 10419 (1992).
[43] J.-i. Igarashi and P. Fulde, Phys. Rev. B **45**, 12357 (1992).
[44] C. Jayaprakash, H. R. Krishnamurthy, and S. Sarker, Phys. Rev. B **40**, 2610 (1989).
[45] S. Sarker, C. Jayaprakash, H. R. Krishnamurthy, and W. Wenzel, Phys. Rev. B **43**, 8775 (1991).
[46] H. J. Schulz, Phys. Rev. Lett. **64**, 1445 (1990).
[47] H. J. Schulz, J. Phys. France **50**, 2833 (1989).
[48] D. Poilblanc and T. M. Rice, Phys. Rev. B **39**, 9749 (1989).
[49] J. Zaanen and O. Gunnarsson, Phys. Rev. B **40**, 7391 (1989).
[50] H. Chu, Solid State Commun. **80**, 1003 (1991).
[51] J. Yang and W. P. Su, Phys. Rev. B **44**, 6838 (1991).
[52] M. Ichimura, M. Fujita, and K. Nakao, J. Phys. Soc. Jpn. **61**, 2027 (1992).
[53] A. V. Chubukov and K. A. Musaelian, Phys. Rev. B **51**, 12605 (1995).
[54] M. Inui and P. B. Littlewood, Phys. Rev. B **44**, 4415 (1991).

[55] M. Dzierzawa, Z. Phys. B: Condens. Matter **86**, 49 (1992).
[56] T. Giamarchi and C. Lhuillier, Phys. Rev. B **42**, 10641 (1990).
[57] T. Dombre, J. Phys. France **51**, 847 (1990).
[58] M. Kato, K. Machida, H. Nakanishi, and M. Fujita, J. Phys. Soc. Jpn. **59**, 1047 (1990).
[59] M. Dzierzawa and R. Frésard, Z. Phys. B: Condens. Matter **91**, 245 (1993).
[60] R. Frésard, M. Dzierzawa, and P. Wölfle, Europhys. Lett. **15**, 325 (1991).
[61] E. Arrigoni and G. C. Strinati, Phys. Rev. B **44**, 7455 (1991).
[62] D. Góra, K. Rościszewski, and A. M. Oleś, Phys. Rev. B **60**, 7429 (1999).
[63] J. Xu, C.-C. Chang, E. J. Walter, and S. Zhang, J. Phys.: Condens. Matter **23**, 505601 (2011).
[64] J. Bonča, J. E. Gubernatis, M. Guerrero, E. Jeckelmann, and S. R. White, Phys. Rev. B **61**, 3251 (2000).
[65] S. R. White and D. J. Scalapino, Phys. Rev. Lett. **91**, 136403 (2003).
[66] G. Hager, G. Wellein, E. Jeckelmann, and H. Fehske, in *High Performance Computing in Science and Engineering, Munich 2004*, edited by S. Wagner, W. Hanke, A. Bode, and F. Durst (Springer, Berlin, 2005), pp. 339–347.
[67] H. Fehske, G. Hager, G. Wellein, and E. Jeckelmann, Physica B **378–380**, 319 (2006).
[68] M. Machida, M. Okumura, S. Yamada, Y. Ohashi, and H. Matsumoto, J. Supercond. Novel Magn. **22**, 275 (2009).
[69] C.-C. Chang and S. Zhang, Phys. Rev. Lett. **104**, 116402 (2010).